Mineralogical Magazine, December 2004, Vol. 68(6), pp. 839–852

Seismic-frequency attenuation at first-order phase transitions: dynamical mechanical analysis of pure and Ca-doped lead orthophosphate

R. J. HARRISON[1,*], S. A. T. REDFERN[1] AND U. BISMAYER[2]

[1] Department of Earth Sciences, University of Cambridge, Downing Street, Cambridge CB2 3EQ, UK
[2] Mineralogisch-Petrographisches Institut, Universität Hamburg, Grindelallee 48, D-20146 Hamburg, Germany

ABSTRACT

The low-frequency mechanical properties of pure and Ca-doped lead orthophosphate, $(Pb_{1-x}Ca_x)_3(PO_4)_2$, have been studied using simultaneous dynamical mechanical analysis, X-ray diffraction (XRD), and optical video microscopy in the vicinity of the first-order ferroelastic phase transition. Both samples show mechanical softening at $T > T_c$, which is attributed to the presence of dynamic short-range order and microdomains. Stress-induced nucleation of the low-temperature ferroelastic phase within the high-temperature paraelastic phase was observed directly via optical microscopy at $T \approx T_c$. Phase coexistence is associated with rapid mechanical softening and a peak in attenuation, P1, that varies systematically with heating rate and measuring frequency. A second peak, P2, occurs $\approx 3-5$ºC below T_c, accompanied by a rapid drop in the rate of mechanical softening. This is attributed to the change in mode of anelastic response from the displacement of the paraelastic/ferroelastic phase interface to the displacement of domain walls within the ferroelastic phase. Both the advancement/retraction of needles (W walls) and wall translation/rotation (W′ walls) modes of anelastic response were identified by optical microscopy and XRD. A third peak, P3, occurring ≈ 15ºC below T_c, is attributed to the freezing-out of local flip disorder within the coarse ferroelastic domains. A fourth peak, P4, occurs at a temperature determined by the amplitude of the dynamic force. This peak is attributed to the crossover between the saturation (high temperature) and the superelastic (low temperature) regimes. Both samples display large superelastic softening due to domain wall sliding in the ferroelastic phase. Softening factors of 20 and 5 are observed in the pure and doped samples, respectively, suggesting that there is a significant increase in the intrinsic elastic constants (and hence the restoring force on a displaced domain wall) with increasing Ca content. No evidence for domain freezing was observed down to -150ºC in either sample, although a pronounced peak in attenuation, P5, at $T \approx -100$ºC is tentatively attributed to the interaction between domain walls and lattice defects.

Both samples show similar high values of attenuation within the domain-wall sliding regime. It is concluded that the magnitude of attenuation for ferroelastic materials in this regime is determined by the intrinsic energy dissipation caused by the wall-phonon interaction, and not by the presence of lattice defects. This will have a large impact on attempts to predict the effect of domain walls on seismic properties of mantle minerals at high temperature and pressure.

KEYWORDS: lead orthophosphate, seismic-frequency attenuation, mechanical properties.

Introduction

THE attenuation of seismic waves is caused by the anelastic (i.e. time-dependent) response of rocks and minerals to an applied stress, resulting in the dissipation of elastic energy. A number of recent studies have highlighted the importance of transformation twinning as a source of anelasticity in ferroelastic materials subjected to alternating stress at seismic frequencies (Harrison and Redfern, 2002; Harrison *et al*., 2003, 2004*a*,*b*).

* E-mail: rjh40@esc.cam.ac.uk
DOI: 10.1180/0026461046860226

Transformation twins form spontaneously on cooling through a paraelastic-ferroelastic phase transition. Each twin domain represents a degenerate orientational variant of the spontaneous strain of the ferroelastic phase. The degeneracy is broken by application of a stress, causing growth of energetically favourable domains at the expense of energetically unfavourable domains. This is achieved by the movement of domain walls. Displacement of domain walls thus results in a time-dependent macroscopic strain, potentially accompanied by massive mechanical softening and very large mechanical attenuation.

Here we apply simultaneous dynamical mechanical analysis, XRD and optical microscopy to study seismic-frequency attenuation at the ferroelastic phase transition in pure and Ca-doped lead orthophosphate $(Pb_{1-x}Ca_x)_3(PO_4)_2$. This study addresses several issues regarding transformation microstructures and anelasticity. Firstly, what effect do substitutional impurity atoms have on the mobility of domain walls and the magnitude of attenuation? It is postulated that substitutional impurities could create lattice strain which would hinder the passage of domain walls and enhance attenuation. Secondly, the phase transition in lead orthophosphate is first order rather than second order. First-order phase transitions are characterized by a structural discontinuity at T_c and a small temperature interval over which the high- and low-temperature phases coexist. Displacement of an interface between coexisting phases is a potential source of attenuation close to any first-order phase boundary (irrespective of whether the transition is displacive, reconstructive, or martensitic in character), and may therefore be relevant to the origin of attenuation in the transition zone, in the vicinity of transitions between the α, β and γ polymorphs of Mg_2SiO_4. Finally, previous measurements of attenuation in oxides with the perovskite structure have been dominated by a large relaxation peak associated with the interaction between domain walls and lattice defects (domain freezing). However, calculations indicate that perovskite in the lower mantle may be far from the domain-freezing regime (Harrison and Redfern, 2002). Hence it is crucial to determine what other factors contribute to the attenuation generated by transformation microstructures. Lead orthophosphate shows no domain freezing above room temperature, allowing the intrinsic energy dissipation due to domain-wall motion to be measured.

Crystallographic details

Phase transition in $Pb_3(PO_4)_2$

The paraelastic-ferroelastic transition in $Pb_3(PO_4)_2$ displays two distinct features. Firstly, strong short-range order exists at $T > T_c$, leading to microdomains with lifetimes on the phonon time scale in crystals of high chemical purity. These microdomains first appear below 260ºC, and are associated with displacement of Pb atoms away from the ternary axis and along one of the three binary axes of the rhombohedral phase. The local symmetry is reduced to monoclinic ($C2/c$), but dynamic 'flips' between the three equivalent displacement directions maintain the macroscopic rhombohedral symmetry ($R\bar{3}m$). Impurities (such as Ba, V, As) pin the microdomains creating static, rather than dynamic, short-range order above T_c. The ferroelastic phase transition occurs below 180ºC. The Pb atoms become permanently displaced in one of the three equivalent directions and there are correlated tilts of the PO_4 tetrahedra. The macroscopic symmetry is reduced from $R\bar{3}m$ to $C2/c$ and coarse twin domains form. A third anomaly at ~160ºC has been attributed to the presence of local flip disorder within the coarse ferroelastic domains between 160 and 180ºC (Salje and Wruck, 1983; Salje *et al.*, 1993).

Transformation twinning in $Pb_3(PO_4)_2$

The relationship between the unit cells of the monoclinic and rhombohedral phases is:

$$\begin{pmatrix} a_{\mathrm{mon}} \\ b_{\mathrm{mon}} \\ c_{\mathrm{mon}} \end{pmatrix} = \begin{pmatrix} 1/3 & 2/3 & 2/3 \\ -1 & 0 & 0 \\ -1 & -2 & 0 \end{pmatrix} \begin{pmatrix} a_{\mathrm{hex}} \\ b_{\mathrm{hex}} \\ c_{\mathrm{hex}} \end{pmatrix} \quad (1)$$

where a_{mon} etc. are the lattice parameters of the monoclinic phase and a_{hex} etc. are the lattice parameters of the rhombohedral phase referred to hexagonal axes. The surface of the samples used in this study are parallel to the $(100)_{\mathrm{mon}}$ cleavage plane, which corresponds to the $(001)_{\mathrm{hex}}$ plane of the rhombohedral phase.

The symmetry-breaking spontaneous strain is of the form:

$$e_{ij} = \begin{pmatrix} e_{11} & 0 & e_{13} \\ 0 & -e_{11} & 0 \\ e_{13} & 0 & 0 \end{pmatrix} \quad (2)$$

There are three orientational variants of the spontaneous strain, related by 120º rotation about z_{hex}. Each monoclinic domain retains one out of the three mirror planes and one out the three binary axes of the rhomohedral phase. The other two mirror planes and binary axes become pseudomirror planes and pseudobinary axes in the monoclinic phase, giving rise to two types of ferroelastic domain wall. A W wall forms parallel to the pseudomirror plane and lies in a fixed crystallographic orientation, approximately normal to the $(100)_{mon}$ cleavage surface. A W′ wall forms parallel to the pseudobinary axis (perpendicular to the W wall) and lies at an angle, $\tan\theta = e_{13}/e_{11}$, to the normal to the $(100)_{mon}$ surface (Sapriel, 1975; Bismayer and Salje, 1981). This angle is ~17º at room temperature in pure lead orthophosphate, enabling W and W′ walls to be easily distinguished in the optical microscope under crossed polars (Fig. 1).

The $(100)_{mon}$ surfaces of the three domain states are tilted with respect to each other by a small angle proportional to e_{13}, leading to the zig-zag surface topography previously identified by atomic force microscopy (Bosbach *et al*., 1997). The maximum angle between $(100)_{mon}$ planes on either side of a W wall (calculated for a tilt axis lying parallel to both the wall and the sample surface) is 1.45º at room temperature in pure lead orthophosphate. This angle can be easily measured from the splitting of peaks in an XRD rocking curve (Wruck *et al*., 1994). For a W′ wall this angle is expected to be zero, since the W′ twin law requires that adjacent domains are related by 180º rotation about the tilt axis. The tilt angle measured about an axis that is not parallel to the W′ wall may be non-zero, however.

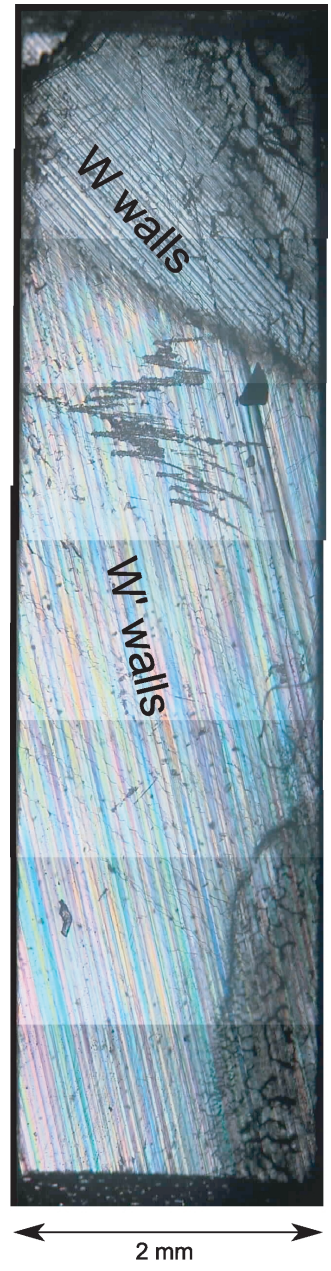

FIG. 1. Optical micrograph of the pure starting material. W walls in the upper portion are perpendicular to the $(100)_{mon}$ cleavage surface and are characterized by the black-white contrast observed when one set of twins is rotated into extinction. W′ walls in the lower portion of the crystal are tilted by an angle of ~17º to the surface and are characterized by their birefringent interference colours.

Experimental procedures

Stroboscopic XRD-DMA

Dynamical mechanical analysis (DMA) is used to determine the anelastic response to an alternating force in three-point bend geometry (Harrison and Redfern, 2002; Harrison *et al*., 2003). The sample is a single crystal beam with length l, width w, and thickness t, suspended on two knife-edges. A force impinges upon the sample from above via a third knife-edge located halfway along the sample length. The applied force has a static component (F_S) and a dynamic component (F_D) with frequency (f) in the range 0.01−50 Hz ($F_D \approx 0.9F_S$). Unless otherwise stated, all measurements have been performed using $f = 1$ Hz. The dynamic

Young's modulus parallel to the sample length is related to the dynamic force and the amplitude of deflection (u_D) via:

$$Y = \frac{l^3}{4t^3 w}\frac{F_D}{u_D}\exp(i\delta) \qquad (3)$$

where δ is the angle by which the deflection lags behind the applied force. The real ($Y' = |Y|\cos\delta$) and imaginary ($Y'' = |Y|\sin\delta$) components of the dynamic modulus are referred to as the storage and loss moduli, respectively. The ratio $Y''/Y' = \tan\delta$ is the attenuation (proportional to the energy dissipated per cycle).

In order to study the dynamic response of the microstructure, a modified DMA has been combined with a stroboscopic X-ray diffractometer, which allows rocking curves to be measured at specific parts of the alternating force cycle (see Harrison *et al*., 2004*a* for a detailed description). The diffractometer comprises an INEL curved position-sensitive detector (PSD), covering 120º2θ, and a sealed-tube X-ray source with monochromator optics and collimation system (Cu-$K\alpha_1$ radiation). A 100 μm diameter beam impinges on the lower surface of the sample, and is diffracted in reflection geometry to the detector. The sample and flexure head components are all enclosed in a thermally-stable furnace with X-ray-transparent windows. For low-temperature measurements the furnace assembly is replaced by a heat sink block in thermal contact with a liquid nitrogen bath.

Rocking curves were collected by setting the angle of the X-ray source to the horizontal (ω) to a value just lower than the Bragg angle (θ) for the $(400)_{mon}$ reflection. The source angle was then increased in steps of 0.005º and diffracted intensity was collected stroboscopically for 30 s per step (effectively 7.5 s for each of the four component rocking curves). At each step, the diffracted intensity as a function of 2θ was integrated using an automated peak-finding and integration routine. Rocking curves are presented as integrated intensity versus ω. There are four individual rocking curves for each measurement, corresponding to the four parts of the dynamic stress cycle: green = minimum force ($F_S - F_D$), red = maximum force ($F_S + F_D$), black = maximum rate of increasing force, blue = maximum rate of decreasing force. High-temperature rocking curves were collected during heating from room-temperature to above T_c and back again. Diffraction measurements were made during a series of isothermal annealing steps under dynamic load. Heating and cooling of the sample between measurements was performed at a rate of approximately 10ºC min^{-1} under dynamic load. The sample remained in the DMA under dynamic load throughout the measurement of each series. A telescopic lens attached to a CCD camera is mounted directly below the sample, allowing the dynamic response of the domain walls to be viewed in reflected light and recorded digitally.

Sample preparation

The pure and Ca-doped lead orthophosphate crystals were synthesized from the following starting materials: PbO (Merck 7401), $(NH_4)H_2(PO_4)$ (Merck 1126) and $CaCO_3$ (Riedel-de-Haen p.A.). Pure lead orthophosphate was first synthesized according to the reaction: $2(NH_4)H_2(PO_4) + 3PbO = Pb_3(PO_4)_2 + 3H_2O + 2NH_3$. Crystals were then grown in closed platinum crucibles using the Czochralski technique. To obtain Ca-doped crystals, the lead phosphate powder was mixed with $CaCO_3$ in stoichiometric proportion and then heated to 1373 K. Crystals were again grown in closed platinum crucibles using the Czochralski technique. The composition $x = 0.025$ was subsequently determined by electron microprobe analysis.

Results

Mechanical properties as a function of temperature

Large changes in storage modulus and tanδ occur as a function of temperature in both the pure and doped samples (Fig. 2). The most rapid change in storage modulus occurs at the ferroelastic transition temperature, T_c, arbitrarily defined here as the temperature at which the modulus is reduced to half its high-temperature value, which also corresponds to the point at which the rate of change of modulus is a maximum. For the pure sample (Fig. 2*a*) the transition occurs at 206ºC. The discrepancy between this and the expected T_c of 180ºC is caused by thermal lag between the furnace and sample when measurements are made using relatively fast heating rates (10ºC/min in this case). A more reliable determination of T_c = 182±0.5ºC was obtained from isothermal measurements very close to the transition. For the doped sample (Fig. 2*b*) the transition occurs at 226ºC (heating rate of 5ºC/min). A more reliable

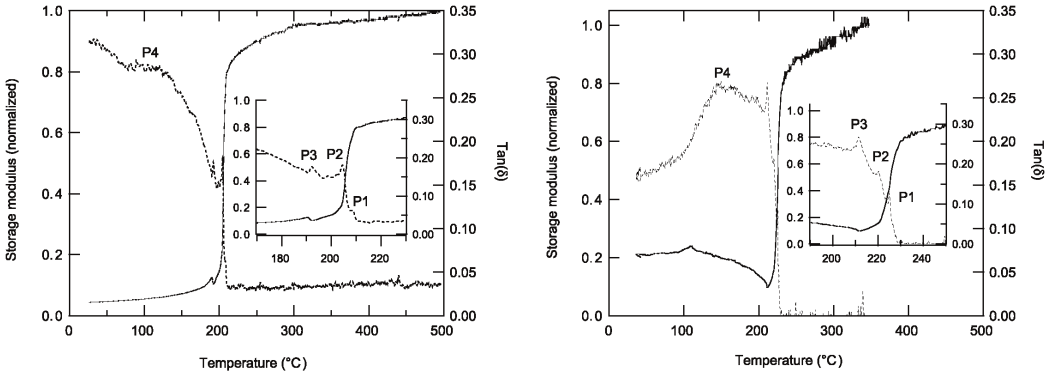

FIG. 2. Normalized storage modulus (solid curves) and tanδ (dashed curves) as a function of temperature. (*a*) Pure sample with $f = 1$ Hz, F_S:F_D = 100:90 mN, and $\dot{T}$ = 10ºC/min. (*b*) 2.5% Ca-doped sample with $f = 1$ Hz, F_S:F_D = 50:45 mN, and $\dot{T}$ = 5ºC/min.

determination of T_c = 207±1.5ºC was obtained from the average of heating and cooling runs at 1ºC/min.

Both the pure and doped samples show evidence of mechanical softening within the paraelastic phase immediately above the transition ($T > T_c$). The pure sample, for example, shows a 20% reduction in modulus on cooling from 500ºC to 210ºC (just above the onset of the phase transition). Softening above T_c can be attributed to the presence of coupling between strain and order-parameter fluctuations (Carpenter and Salje, 1998; Redfern *et al*., 2004). The softening appears to accelerate below 300ºC, and may, therefore, be associated with the presence of dynamic short-range order and microdomains.

The behaviour of the pure and doped samples close to the transition is very similar (see insets in Fig. 2). The onset of the phase transition on cooling is clearly seen as a sudden increase in the rate of softening (~60% decrease in modulus over a temperature interval of ~6ºC) and a corresponding peak, P1, in tanδ. This is followed by a sudden decrease in the rate of softening and a second peak, P2, in tanδ. Around 15ºC below P1 there is a small but sudden increase in the storage modulus and a third peak, P3, in tanδ. On further cooling, the behaviour of the pure and doped samples diverges. In the pure sample, the modulus typically decreases with decreasing temperature, reaching room-temperature value that is 5% of that measured at 500ºC (softening by a factor of 20). In the doped sample, the modulus typically increases with decreasing temperature, reaching a room-temperature value that is 20% of that measured at 300ºC (softening by a factor of 5). In both samples tanδ typically increases with decreasing temperature, reaching a small peak or plateaux, P4.

Neither sample shows evidence of domain freezing down to room temperature. Preliminary measurements below room temperature, however, reveal the presence of a pronounced peak, P5, in tanδ at −100ºC (Fig. 3). This peak is accompanied by small and gradual increases in modulus, rather than the large and rapid increase that is observed in $LaAlO_3$ and $(Ca,Sr)TiO_3$ (Harrison and Redfern, 2002; Harrison *et al*., 2003;, 2004*b*). This implies that a significant proportion of domain walls remain mobile below −100ºC. The origin of this peak requires further investigation, but is probably related to the interaction between domain walls and lattice defects. The origin of peaks P1−P4 is explored further below.

Mechanical properties as a function of force

The mechanical properties of a ferroelastic material vary greatly with the amplitude of dynamic force (Harrison and Redfern, 2002). Plots of the dynamic force amplitude (F_D) versus dynamic deflection amplitude (u_D) are shown in Fig. 4 for the pure lead orthophosphate sample. At $T > T_c$ (the paraelastic regime), the force-deflection plots are straight lines passing through the origin. This corresponds to a normal linear mechanical response with dF_D/du_D proportional to the storage modulus (equation 3). The maximum force and deflection values at $T > T_c$ correspond to stress and strain values of 1.1 MPa and 3.6×10^{-4}, respectively, and a modulus of

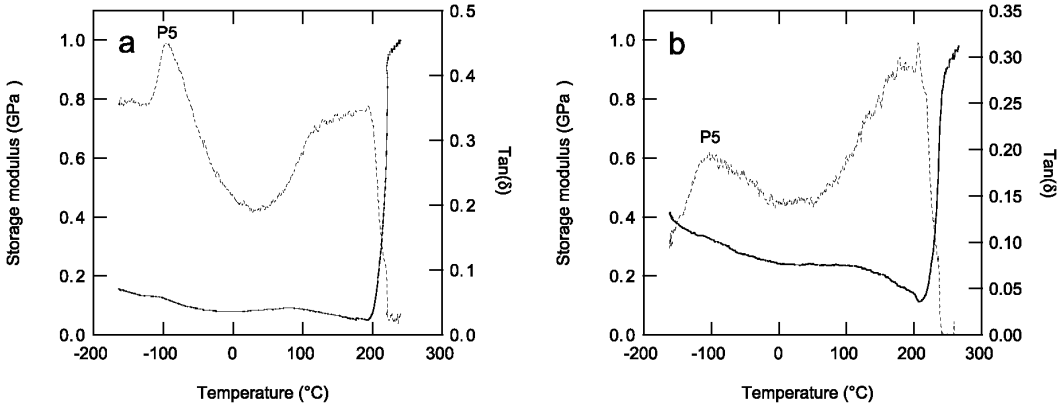

FIG. 3. Normalized storage modulus (solid curves) and tanδ (dashed curves) measured at low temperatures using a liquid N_2 bath. (*a*) Pure sample with $f = 1$ Hz, F_S:F_D = 50:45 mN, and $\dot{T} = 10$ºC/min. (*b*) 2.5% Ca-doped sample with $f = 1$ Hz, F_S:F_D = 50:45 mN, and $\dot{T} = 10$ºC/min. Both samples show a peak in tanδ around −100ºC. The relatively small increase in modulus accompanying the peak indicates that a significant proportion of walls remain mobile below −100ºC.

3 GPa. Non-linear behaviour is observed at $T < T_c$ (Harrison and Redfern, 2002; Harrison *et al*., 2004*b*). For $F_D < 25$ mN, the force-deflection curves are essentially linear and coincident. The slope dF_D/du_D is a factor of 30 lower than that of the paraelastic regime. This massive mechanical softening occurs because the macroscopic strain is accommodated by the displacement of domain walls, rather than by distortion of the lattice (the superelastic regime). The maximum force and deflection values at $T < T_c$ correspond to maximum stress and strain values of 1.1 MPa

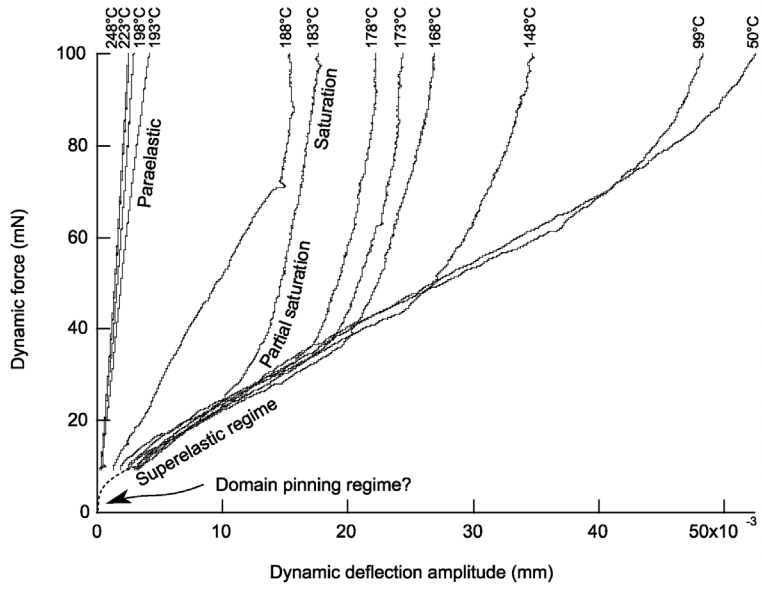

FIG. 4. Dynamic force, F_D (mN), *vs*. dynamic deflection, u_D (mm), in the pure sample for a range of temperatures. The linear trend established in the superelastic regime extrapolates to a positive value of $F_D = 5-10$ mN at $u_D = 0$, indicating that a critical force is required to initiate domain wall motion. The domain wall pinning regime is expected to occur for forces lower than this (indicated schematically by the dashed line).

and 7.2×10^{-3}, respectively, and a modulus of 0.15 GPa. Domain walls displace by an equilibrium amount determined by the balance between a driving force (provided by the applied stress) and a restoring force (determined by wall-wall, wall-surface, and wall-defect interactions). The macroscopic strain for a given wall displacement is directly proportional to the spontaneous strain, whereas the amount of displacement is inversely proportional to the spontaneous strain (i.e. walls move further when the spontaneous strain is lower). The net result is that the macroscopic strain is independent of the spontaneous strain and, therefore, independent of temperature (Harrison and Redfern, 2002). This explains why all force-deflection curves are coincident within the superelastic regime, and why the decrease in modulus below T_c is so rapid.

Harrison *et al*. (2004*a*) identified two modes of anelastic response in ferroelastic crystals. The first mode involves rapid advancement/retraction of needle domains. With increasing F_D, there comes a point when the equilibrium distance moved by the needle tips is greater than the sample width. At this point the macroscopic strain is no longer independent of the spontaneous strain and there is a sudden increase in dF_D/du_D, marking the beginning of the partial saturation regime. Partial saturation occurs when there is a range of distances over which needles are free to move and/or a range of domain-wall mobilities, so that only a fraction of the available needle tips reach the sample edge during the dynamic force cycle. The force needed to enter the partial saturation regime varies with temperature, with $F_D \approx 25$ mN at 183ºC and $F_D \approx 80$ mN at 50ºC. This is a consequence of the fact that domain walls displace more when the spontaneous strain is low, so that saturation occurs at lower forces for temperatures close to T_c. For a given value of F_D, one expects a crossover between the superelastic and partial saturation regimes to occur at a distinct temperature. Furthermore, this crossover temperature should increase with decreasing F_D. This effect is illustrated in Fig. 5, which compares temperature scans of the doped sample acquired at two different force levels. The position of the peak P4 in tanδ shifts from 156ºC at 50:45 mN to 179ºC at 20:18 mN. This provides compelling evidence that the origin of P4 is a crossover between superelastic and partial saturation regimes.

With increasing F_D, the fraction of saturating needles increases and dF_D/du_D approaches that of

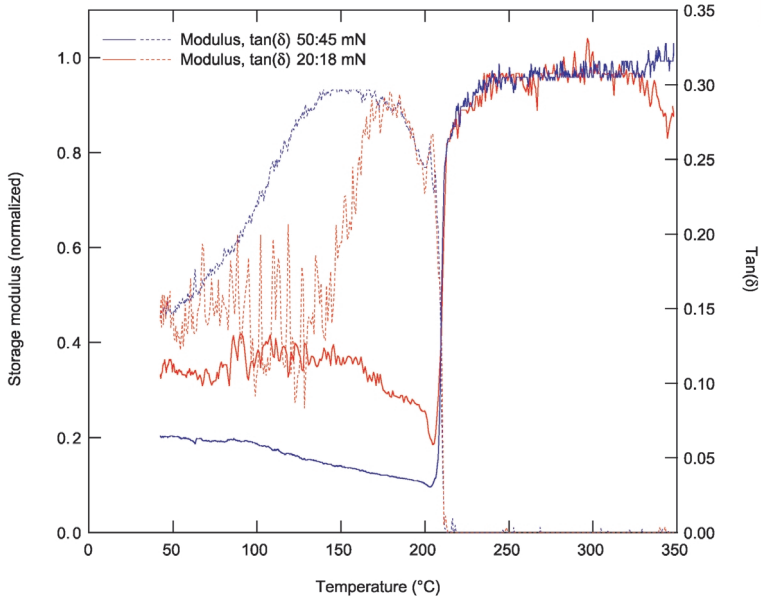

FIG. 5. Comparison of storage modulus (solid curves) and tanδ (dashed curves) *vs*. temperature at different applied forces (2.5% Ca-doped sample). Blue curves were collected using F_S:F_D = 50:45 mN, f = 1 Hz, $\dot{T} = -5$ºC/min. Red curves were collected using F_S:F_D = 20:18 mN, f = 1 Hz, $\dot{T} = -5$ºC/min. Note shift in position of P4 with changing force.

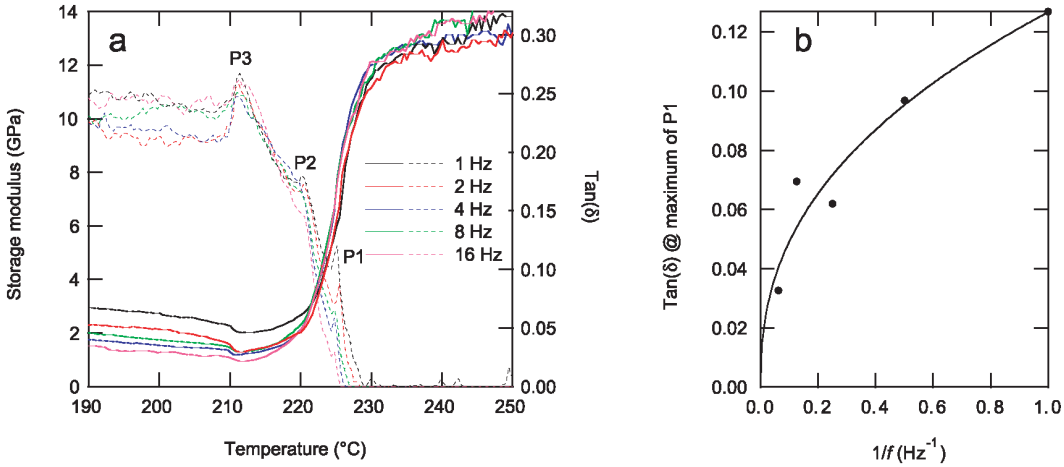

FIG. 6. (*a*) Comparison of storage modulus (solid curves) and tanδ (dashed curves) *vs*. temperature at different applied frequencies (2.5% Ca-doped sample, F_S:F_D = 50:45 mN, $\dot{T}$ = 5ºC/min). (*b*) Height of peak P1 as a function of inverse frequency (solid circles). Curve is a least squares fit to the data using tanδ = $a(1/f)^n$, with a = 0.13 and n = 0.4.

the paraelastic regime. Full saturation can only occur when both modes of anelastic response are saturated. The second mode identified by Harrison *et al*. (2004*a*) involves the lateral translation of lamellar twin walls. Three-point-bend geometry requires that domain walls move in opposite directions at the top and bottom surfaces of the sample, resulting in rotation, rather than translation, of the domain wall. Adjacent walls rotate in opposite senses, so that for sufficient values of F_D they come into contact at the top and bottom surfaces, causing saturation.

The linear relationship between force and deflection in the superelastic regime extrapolates to a positive value of F_D = 5−10 mN at u_D = 0. This corresponds to the critical dynamic force required to initiate domain-wall motion. Similar values were obtained for the doped sample. Values of F_D below this critical threshold are insufficient to rip domain walls away from their pinning sites (the domain wall pinning regime). Enhanced pinning of domain walls may explain the significant decrease in the overall degree of softening when small forces are used (Fig. 5).

Attenuation at T close to T_c

To further investigate the origins of peaks P1, P2 and P3, temperature scans were acquired for the doped sample at a range of frequencies, f, and heating rates, $\dot{T}$ (Figs 6 and 7). The positions of all three peaks are independent of f (Fig. 6*a*), demonstrating that they are not caused by relaxation processes (Harrison *et al*., 2004*b*). The height of P1 decreases with increasing f (Fig. 6*b*) and increases with increasing $\dot{T}$ (Fig. 7). This is typical of the behaviour associated with the coexistence of high-temperature and low-temperature phases close to T_c (Wang *et al*., 2000; Zhang *et al*., 1995*a*,*b*; Pérez-Sáez *et al*., 1998). Phase coexistence at first-order phase transitions leads to a transient contribution to the attenuation proportional to $(\dot{T}/f)^n$ (Zhang *et al*., 1995*a*; Wang *et al*., 2000). For a fixed $\dot{T}$, the height of P1 is

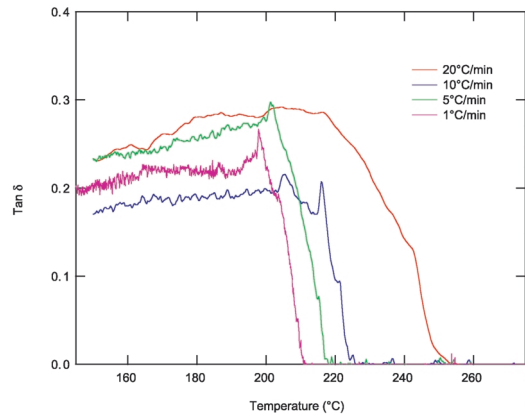

FIG. 7. Comparison of tanδ (solid curves) *vs*. temperature at different heating rates (2.5% Ca-doped sample, F_S:F_D = 50:45 mN, f = 1 Hz). Dashed line is a guide to the eye, indicating the increase in height of peak P1 with increasing heating rate.

proportional to $(1/f)^n$ with $n = 0.4$ (solid line in Fig. 7). Direct confirmation that P1 is caused by stress-induced nucleation of the low-temperature phase within the high-temperature phase was obtained using *in situ* optical observation (Fig. 8; movie available online: ftp://www.esc.cam.ac.uk/pub/rjh40/). The transition begins on cooling from $T > T_c$ with the formation of needles of the low-temperature phase at the central knife-edge. These spread into the surrounding high-temperature phase as the applied force increases, and denucleate when the force is reduced to a minimum. The amount of low-temperature phase produced during each cycle increases on cooling until the entire sample is monoclinic and the macroscopic strain is accommodated by domain wall displacement rather than displacement of the phase interface. This change in mode of anelastic response coincides with peak P2 and the sudden drop in the rate of softening.

No obvious change in microstructure could be correlated with peak P3, which occurs ~15ºC below T_c. This peak, and the corresponding increase in modulus, may be associated with the freezing out of local flip disorder within the ferroelastic domains, which is observed ~20ºC below T_c using differential scanning calorimetry and XRD measurements (Salje and Wruck, 1983; Salje *et al*., 1993).

Stroboscopic XRD-DMA

A sequence of stroboscopic rocking curves was collected for the doped sample on heating and cooling through the transition (Fig. 9). The microstructure of the starting crystal consisted of closely-spaced W walls at an angle of ~82º to the sample length. The room temperature rocking curve (bottom of Fig. 9*a*) contains a broad asymmetric peak at the minimum applied force (green curve) and a broader, more symmetric, peak at the maximum applied force (red curve). The two peaks are shifted with respect to each other by $\Delta\omega = 0.25º$. The expected rocking angle between $(400)_{mon}$ planes in adjacent domains separated by a W wall is:

$$\Delta\omega = \Delta\omega_{max}\sin\phi \qquad (4)$$

where ϕ is the angle between the incident X-ray beam and the trace of the domain wall on the surface and $\Delta\omega_{max}$ is the maximum tilt angle between $(400)_{mon}$ planes in the two domains (Harrison *et al*., 2004*a*). Assuming $\Delta\omega_{max} = 1.45º$ for doped lead orthophosphate (i.e. the same value

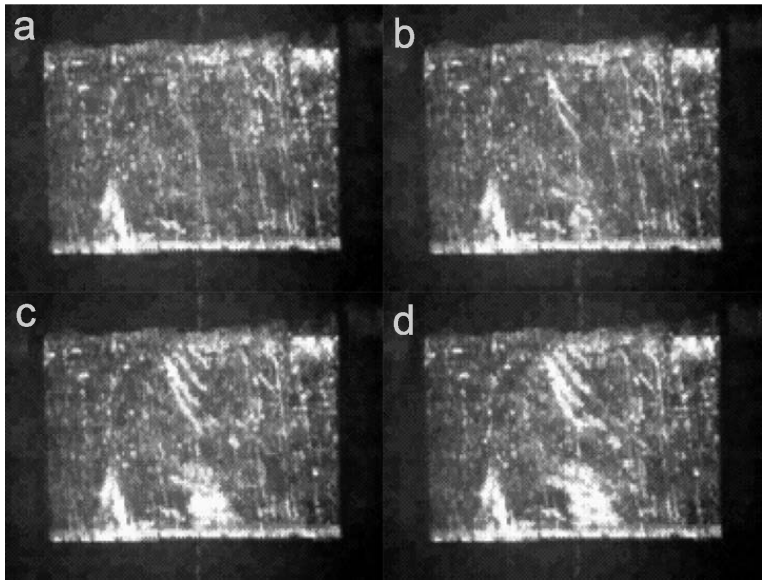

FIG. 8. (Movie available online: ftp://www.esc.cam.ac.uk/pub/rjh40/). Snapshots of microstructure observed as a function of force in reflected light at $T \approx T_c$. Applied force increases in the order a → b → c → d. Nucleation of needle twins at the central knife edge is observed (*b*). These then grow into the crystal with increasing force (*c* and *d*). Twins denucleate when force is released.

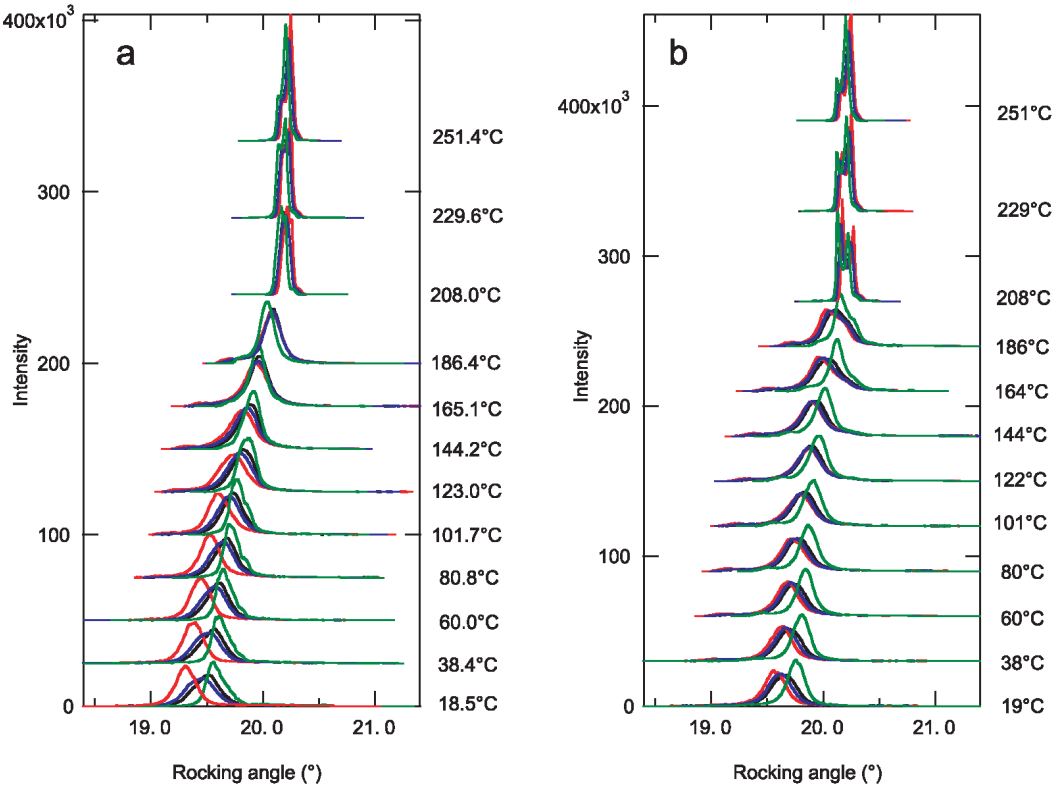

FIG. 9. Stroboscopic XRD rocking curves as a function of temperature for the 2.5% Ca-doped sample, recorded at 1 Hz and 300:270 mN. Data collected on (*a*) heating and (*b*) cooling. The four components of the rocking curve correspond to different parts of the dynamic stress cycle: green line = minimum force (30 mN), redline = maximum force (570 mN), black line = maximum rate of increasing force, blue line = maximum rate of decreasing force.

as pure lead orthophosphate), a rocking angle of 0.25º yields $\phi = 9.9º$, which is consistent with the observed angle between W walls and the X-ray beam in the starting material (allowing for the possibility of an ~2º misorientation of the sample on the knife edges). The simplest interpretation of the rocking curves, therefore, is that alternate domain states are being probed by diffraction at the maximum and minimum parts of the force cycle (i.e. the domain wall separating adjacent domains tracks back and forth across the X-ray beam during the force cycle). The observed values of $\Delta\omega$ as a function of temperature are compared with values calculated from the high-temperature lattice parameters of pure lead orthophosphate (Salje *et al*., 1993) in Fig. 10. Below 180ºC there is good agreement between observed and calculated values (considering the difference in T_c between the pure and doped samples). The change in sign of the observed splitting above 180ºC probably reflects the intrinsic shift in peak position due to elastic deflection of the sample in the DMA. The complex form of the rocking curve peaks above T_c is caused by imperfections in the sample surface.

On cooling (Fig. 9*b*), $\Delta\omega$ remains roughly constant with temperature below the transition, indicating a change in microstructure and/or mode of anelastic response. Optical micrographs of the sample after completion of the cooling runs confirmed that the microstructure close to the centre of the sample had changed from W walls at ~82º to the sample length to W′ walls at ~40º to the sample length. The behaviour of the rocking curves is similar to that observed in $LaAlO_3$, and suggests that the mode of anelastic response has changed to lateral translation/rotation of W′ walls, rather than advancement/retraction of W needles.

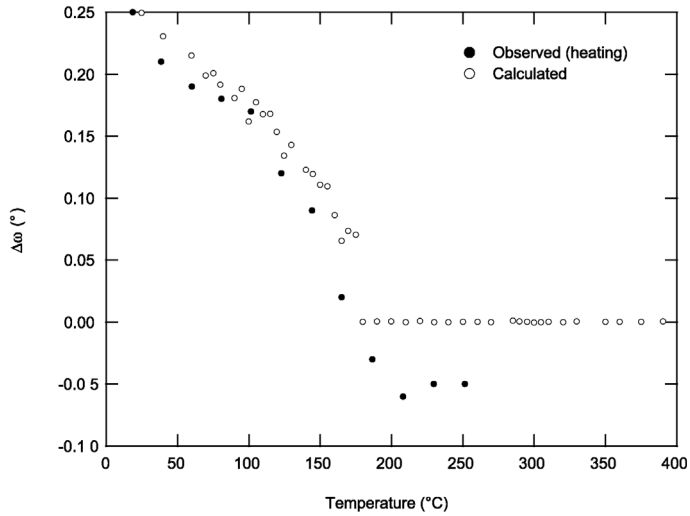

FIG. 10. Comparison of observed *vs*. calculated angle between rocking curve peaks for two domains separated by a W wall. Observed values (closed circles) were determined from this angle between peaks at the maximum and minimum applied force for the 2.5% Ca-doped sample (green and red curves in Fig. 9*a*). Calculated values (open circles) were determined from the high-temperature lattice parameters of pure lead phosphate (Salje *et al*., 1993), assuming $\phi = 9.9^{o}$ (equation 4).

Discussion

What determines attenuation far from the domain wall pinning regime?

In our previous studies of domain-wall anelasticity of ferroelastic oxides, the attenuation was dominated by a large relaxation peak associated with the pinning of domain walls by lattice defects (Harrison and Redfern, 2002; Harrison *et al*., 2003, 2004*a*,*b*). The present experiments have been conducted far away from the domain-wall pinning regime, yet the magnitude of attenuation is still very high. This implies that there is a large intrinsic energy dissipation due to moving domain walls through the lattice. Indeed, the presence of unexpectedly high attenuation well away from the domain-wall pinning regime was noted previously for $LaAlO_3$ and $(Ca,Sr)TiO_3$ (Harrison and Redfern, 2002; Harrison *et al*., 2003). Understanding the intrinsic energy dissipation due to domain wall-motion is essential if we are to understand the contribution to attenuation from domain walls in minerals at high temperature and pressure.

The equation of motion for a domain wall can be written (Huang *et al*., 1992; Wang *et al*., 1996; Combs and Yip, 1983):

$$F_C - \frac{dU(x)}{dx} + F_I - \Gamma x\dot{T} = MX\ddot{T} \qquad (5)$$

where x is the position and M is the effective mass per unit area of the wall. F_C is the configuration force, i.e. the driving force per unit area for wall motion:

$$F_C = \sigma''(e''_A - e''_A) \qquad (6)$$

where σ'' is the applied stress parallel to the sample length and e''_A and e''_B are the components of spontaneous strain in adjacent domains A and B. $U(x)$ is a potential energy describing both the periodic variation in wall energy due to the discreteness of the lattice (Peierls barrier) and the random fluctuations in wall energy due to the presence of defects. In the domain sliding regime (i.e. for forces larger than the critical unpinning force), $U(x)$ causes oscillations in the velocity of the propagating wall. In the domain pinning regime (i.e. for forces closer to the critical unpinning force), $U(x)$ can lead to trapping of walls. F_I is the interaction force between adjacent domain walls (Huang *et al*., 1992):

$$F_I = -2CNe^2x = -kx \qquad (7)$$

where C is an elastic constant, N is the number of domain walls per unit length, and e is the spontaneous strain. Equation 7 provides the restoring force that determines how far domain walls displace under an applied stress. Harrison and Redfern (2002) formulated this force in terms

of the lattice compatibility condition for a rotating wall, which is also proportional to e^2. γ is a viscous friction coefficient resulting from wall-phonon interactions (Combs and Yip, 1983).

In the absence of a restoring force, and assuming we are well within the domain sliding regime (so the effect of $U(x)$ can be ignored), the velocity of the domain wall under a given stress is simply (e.g. Nattermann *et al*., 2001):

$$x\dot{T} = \frac{1}{\Gamma}\sigma''(e''_{\mathrm{A}} - e''_{\mathrm{B}}) \tag{8}$$

In the presence of a restoring force (either due to wall-wall interactions or lattice incompatibility), the wall is expected to come to rest after a certain equilibrium displacement, x_{eq}. In this case both $x\dot{T}$ and $x\ddot{T}$ in equation 5 vanish, yielding:

$$x_{\mathrm{eq}} = \frac{\sigma''(e''_{\mathrm{A}} - e''_{\mathrm{B}})}{k} \tag{9}$$

Equation 9 is valid only within the superelastic regime (i.e. for x_{eq} less than the dimensions of the sample and less than the distance between adjacent walls). The macroscopic strain created by this wall displacement is (Harrison and Redfern, 2002):

$$e'' = N(e''_{\mathrm{A}} - e''_{\mathrm{B}})x_{\mathrm{eq}} \tag{8}$$

Combining equations 7, 9 and 10, and substituting $\mathrm{e}''_{\mathrm{A}} - \mathrm{e}''_{\mathrm{B}} = f(a_{\mathrm{ij}})e$, where $f(a_{\mathrm{ij}})$ is a function of the direction cosines describing the orientation of applied stress relative to the crystallographic axes (Harrison and Redfern, 2002; Harrison *et al*., 2003), the storage modulus in the superelastic regime is:

$$Y = \frac{\sigma''}{e''} = \frac{2C}{f(a_{\mathrm{ij}})^2} \tag{11}$$

Note that the modulus is independent of the spontaneous strain and therefore independent of temperature, as observed (Fig. 4). For an alternating stress, the attenuation is (Wang *et al*., 1996):

$$\tan\delta = \frac{1}{JC}\frac{\omega\tau}{1+\omega^2\tau^2} \tag{12}$$

where $\tau = \Gamma/k$ (i.e. the time needed to travel a distance x_{eq} at a velocity given by equation 8) and J is the intrinsic elastic compliance of the lattice.

The microscopic origin of Γ has been investigated by computer simulation (Combs and Yip, 1983, 1984; Kunz and Combs, 1985). This term arises when the discrete nature of the lattice and wall are taken into account, and becomes zero in the continuum limit. As the wall propagates, lattice fluctuations are generated in its wake. This 'phonon radiation' is the primary mechanism of energy dissipation. The 'zero-temperature' magnitude of γ was obtained from the simulations:

$$\Gamma = \mathrm{A}\exp\left(-\frac{\mathrm{B}w^2}{2}\right) \tag{13}$$

where A and B are constants and w is the width of a wall with profile $\tanh(x/w)$. Variations in γ as a function of temperature were identified via molecular dynamics simulation (Combs and Yip, 1984) although the precise form of these variations remains unclear. According to equation 13, one might expect the temperature dependence of Γ to be determined by the temperature variation in the wall width. The effect of changing wall width, wall density, and spontaneous strain on the relaxation time ($\tau = \Gamma/k$) leads to complex behaviour in the vicinity of T_{c} (Huang *et al*., 1992).

From this analysis it is clear that determining the magnitude of Γ is key to estimating the magnitude of attenuation in the domain sliding regime. Combs and Yip (1984) demonstrate how, for a model one-dimensional system, Γ can be determined from the Fourier transform of the velocity autocorrelation function for a self-diffusing domain wall, obtained through molecular dynamics simulation. Extension of this approach to three-dimensional crystal structures at high pressure and temperature would be a significant step towards an understanding of domain-wall mobility in mantle minerals. Qualitatively, Γ is expected to be large when the width of the wall is only a small multiple of the lattice spacing. Wall widths of 10–20 lattice spacing are sufficient to generate high attenuation in the one-dimensional simulations of Combs and Yip (1983). Similar widths are observed in a wide range of ferroelastic materials (Chrosch and Salje, 1999), including lead orthophosphate (Wruck *et al*., 1994; Bismayer *et al*., 2000).

Effect of impurities

The initial hypothesis, that the presence of Ca impurities would hinder domain wall motion and

enhance attenuation, is not fully supported by the experimental observations (Figs 2 and 3). Although the magnitude of superelastic softening in the doped sample is generally less than that of the pure sample, the magnitude of attenuation is unaffected. The analysis of the previous section indicates that in the domain-sliding regime the magnitude of mechanical softening is determined primarily by the restoring force constant, k (equations 7 and 11), whereas the velocity and energy dissipation of a moving wall are primarily controlled by the wall-phonon interaction parameter, Γ (equations 8 and 12). The defect potential, $U(x)$, in equation 6 induces small oscillatory perturbations in wall velocity, which have little impact on the overall mechanical properties (Combs and Yip, 1983). The experimental observations may be explained if doping has little effect on the wall-phonon interaction but a significant impact on the elastic constant, C, in equation 7. It is also important to compare the average distance between Ca atoms with the typical width of domain walls in lead orthophosphate. For 2.5% substitution, a $2 \times 2 \times 2$ supercell of the monoclinic phase (containing 96 Pb atoms) would contain 2–3 Ca atoms, with average separation <20 Å. This is well below the room temperature width of a domain wall in lead orthophosphate (~60 Å; Wruck *et al*., 1994). In this case the defect contribution to $U(x)$ may be negligible. Experiments on samples with much lower doping levels are now required.

Phase coexistence

A key result of this study is the observation of stress-induced nucleation of a ferroelastic phase from a paraelastic matrix. The preferential nucleation of favourably-oriented twin domains under an applied stress is an effective mechanism of mechanical softening and potent source of attenuation. Such processes will have a bearing on any phase first-order phase transition. For example, the boundary between the transition zone and the lower mantle is defined by the transformation of Mg_2SiO_4 (cubic spinel) to $MgSiO_3$ (orthorhombic perovskite) and MgO. Formation of the orthorhombic perovskite may be influenced by local tectonic or seismic stresses, causing preferential nucleation of certain twin orientations. This would result in enhanced attenuation and lattice-preferred orientation at the transition zone/lower mantle boundary, coupled with anomalously low seismic velocity.

Acknowledgements

The authors would like to thank Ekhard Salje for useful discussions. This work was supported by EPSRC grant GR/M49816 and NERC grant NER/A/S/2003/00537.

References

Bismayer, U. and Salje, E.K.H. (1981) Ferroelastic phases in $Pb_3(PO_4)_2$-$Pb_3(AsO_4)_2$: X-ray and optical experiments. *Acta Crystallographica*, **A37**, 145–153.

Bismayer, U., Mathes, D., Bosbach, D., Putnis, A., van Tendeloo, G., Novak, J. and Salje, E.K.H. (2000) Ferroelastic orientation states and domain walls in lead phosphate type crystals. *Mineralogical Magazine*, **64**, 233–239.

Bosbach, D., Putnis, A., Bismayer, U. and Güttler, B. (1997) An AFM study on ferroelastic domains in lead phosphate, $Pb_3(PO_4)_2$. *Journal of Physics: Condensed Matter*, **9**, 8397–8405.

Carpenter, M.A. and Salje, E.K.H. (1998) Elastic anomalies in minerals due to structural phase transitions. *European Journal of Mineralogy*, **10**, 693–812.

Chrosch, J. and Salje, E.K.H. (1999) Temperature dependence of the domain wall width in $LaAlO_3$. *Journal of Applied Physics*, **85**, 722–727.

Combs, J.A. and Yip, S. (1983) Single-kink dynamics in a one-dimensional atomic chain: A nonlinear atomistic theory and numerical simulation. *Physical Review B*, **28**, 6873–6885.

Combs, J.A. and Yip, S. (1984) Molecular dynamics study of lattice kink diffusion. *Physical Review B*, **29**, 438–445.

Harrison, R.J. and Redfern, S.A.T. (2002) The influence of transformation twins on the seismic-frequency elastic and anelastic properties of perovskite: Dynamical mechanical analysis of single-crystal $LaAlO_3$. *Physics of the Earth and Planetary Interiors*, **134**, 253–272.

Harrison, R.J., Redfern, S.A.T. and Street, J. (2003) The effect of transformation twins on the seismic-frequency mechanical properties of polycrystalline $Ca_{1-x}Sr_xTiO_3$ perovskite. *American Mineralogist*, **88**, 574–582.

Harrison, R.J., Redfern, S.A.T., Buckley, A. and Salje, E.K.H. (2004) Application of real-time, stroboscopic X-ray diffraction with dynamical mechanical analysis to characterise the motion of ferroelastic domain walls. *Journal of Applied Physics*, **95**, 1706–1717.

Harrison, R.J., Redfern, S.A.T. and Salje, E.K.H. (2004) Dynamical excitation and anelastic relaxation of ferroelastic domain walls in $LaAlO_3$. *Physical Review B: Condensed Matter*, **69**, 144101.

Huang, Y.N., Wang, Y.N. and Shen, H.M. (1992) Internal friction and dielectric loss related to domain walls. *Physical Review B*, **46**, 3290–3295.

Kunz, C. and Combs, J.A. (1985) Discrete theory of kink diffusion in the f4 lattice with comparison to the continuum approximation. *Physical Review B*, **31**, 527–535.

Nattermann, T., Pokrovsky, V. and Vinokur, V.M. (2001) Hysteretic dynamics of domain walls at finite temperatures. *Physical Review Letters*, **87**, 197005.

Pérez-Sáez, R.B., Rescarte, V., Nó, M.L. and San Juan, J. (1998) Anelastic contributions and transformed volume fraction during thermoelastic martensitic transformations. *Physical Review B*, **57**, 5684–5692.

Salje, E.K.H. and Wruck, B. (1983) Specific-heat measurements and critical exponents of the ferroelastic phase transition in $Pb_3(PO_4)_2$ and $Pb_3(P_{1-x}As_xO_4)_2$. *Physical Review B*, **28**, 6510–6518.

Salje, E.K.H., Graeme-Barber, A. and Carpenter, M.A. (1993) Lattice parameters, spontaneous strain and phase transitions in $Pb_3(PO_4)_2$. *Acta Crystallographica*, **B49**, 387–392.

Sapriel, J. (1975) Domain-wall orientations in ferroelastics. *Physical Review B*, **12**, 5128–5140.

Wang, Y.N., Huang, Y.N., Shen, H.M. and Zhang, Z.F. (1996) Mechanical and dielectric energy loss related to the viscous motion and freezing of domain walls. *Journal de Physique IV, Colloque C8, supplement to Journal de Physique III*, **6**, 505–514.

Wang, Y.N., Tian, W., Huang, Y.N., Yan, F., Shen, H.M., Zhu, J.S. and Zhang, Z.F. (2000) Mechanical and dielectric dissipation related to phase transitions. *Phase Transitions*, **72**, 57–80.

Wruck, B., Salje, E.K.H., Zhang, M., Abraham, T. and Bismayer, U. (1994) On the thickness of ferroelastic twin walls in lead phosphate $Pb_3(PO_4)_2$. An X-ray diffraction study. *Phase Transitions*, **48**, 135–148.

Zhang, J.X., Fung, P.C.W. and Zeng, W.G. (1995*a*) Dissipation function of the first-order phase transformation in solids via internal-friction measurements. *Physical Review B*, **52**, 268–277.

Zhang, J.X., Yang, Z.H. and Fung, P.C.W. (1995*b*) Dissipation function of the first-order phase transformation in VO_2 ceramics by internal-friction measurements. *Physical Review B*, **52**, 278–284.

[*Manuscript received 1 July 2004: revised 20 October 2004*]